



ORIGINAL ARTICLE

Magnetically recyclable Schiff-based palladium nanocatalyst [Fe₃O₄@SiNSB-Pd] and its catalytic applications in Heck reaction



Hamid Hafizi ^a, Md. Lutfor Rahman ^{b,*}, Mohd Sani Sarjadi ^b,
Mohammed Salim Akhter ^c, Maurice N. Collins ^d, Emmet J. O'Reilly ^a,
Gavin M. Walker ^a, Shaheen M. Sarkar ^{a,e,*}

^a Department of Chemical Sciences, Bernal Institute, University of Limerick, Limerick V94 T9PX, Ireland

^b Faculty of Science and Natural Resources, Universiti Malaysia Sabah, Kota Kinabalu, 88400 Sabah, Malaysia

^c Department of Chemistry, University of Bahrain, Bahrain

^d School of Engineering, Bernal Institute, University of Limerick, Limerick V94 T9PX, Ireland

^e Department of Applied Science, Technological University of the Shannon: Midlands Midwest, Moylish, Limerick V94 EC5T, Ireland

Received 1 December 2021; accepted 10 April 2022

Available online 18 April 2022

KEYWORDS

Magnetic nanoparticles;
Silica coated;
Phenanthroline;
Palladium;
Schiff-base;
Heck reaction

Abstract A magnetically separable palladium nanocatalyst has been synthesized through the immobilization of palladium onto 3-aminopropylphenanthroline Schiff based functionalized silica coated superparamagnetic Fe₃O₄ nanoparticles. The nanocatalyst (Fe₃O₄@SiNSB-Pd) was fully characterized using several spectroscopic techniques, such as FT-IR, HR-SEM, TEM, XRD, ICP, and XPS. The microscopic image of Fe₃O₄ showed spherical shape morphology and had an average size of 150 nm. The Pd-nanoparticles exhibited an average size 3.5 ± 0.6 nm. The successful functionalization of Fe₃O₄@SiNSB-Pd was identified by FT-IR spectroscopy and the appearance of palladium species in Fe₃O₄@SiNSB-Pd was confirmed by XRD analysis. While XPS has been utilized for the determination of the chemical oxidation state of palladium species in Fe₃O₄@SiNSB-Pd. Several activated and deactivated arene halides and olefines were employed for Mizoroki-Heck cross-coupling reactions in the presence of Fe₃O₄@SiNSB-Pd, each of which produced the respective cross-coupling products with excellent yields. The Fe₃O₄@SiNSB-Pd shows good reactivity and reusability for up to seven consecutive cycles.

© 2022 The Author(s). Published by Elsevier B.V. on behalf of King Saud University. This is an open access article under the CC BY-NC-ND license (<http://creativecommons.org/licenses/by-nc-nd/4.0/>).

* Corresponding author.

E-mail addresses: lotfor@ums.edu.my (Md. Lutfor Rahman), shaheen.sarkar@tus.ie (S.M. Sarkar).

Peer review under responsibility of King Saud University.



1. Introduction

In recent decades, the Mizoroki-Heck C-C bond formation reaction of olefins with arene halides or arenediazonium salts has emerged as a novel method for the development of pharmaceuticals, natural products, modern materials, bioactive molecules, and a variety of other derivatives that are used as intermediate compounds in various industries (Trost et al., 2016; Biffis et al., 2018; Arghan et al., 2018; Parouch et al., 2020). Conventional Heck reactions employ highly soluble Pd-phosphine complexes and show high efficiency in cross-coupling reactions (Das et al., 2010; Sardarian et al., 2019; Parlett et al., 2013). The production of highly reactive stable Pd-ligand catalytic systems with minimal Pd leaching is highly desirable for industry, especially in the synthesis of sensitive organic biomolecules, pharmaceuticals, organoelectronic materials and the food industry (Veerakumar et al., 2017). Despite the high reactivity in the catalytic reaction, homogeneous catalytic reactions based on metals still suffer from several disadvantages such as thermal instability and complex and laboriousness process for the separation of the metal catalysts from the reaction mixture and final product. The high cost of the metal and the use of toxic and hazardous solvents limit their further practical application in the development of homogeneous catalysts (Polshettiwar et al., 2011; Esmailpour et al., 2014).

Several organometallic catalysts have been developed for Heck reactions, for example Cu (Calo et al., 2005), Ni (Zheng and Newman, 2019), Co (Kazemnejadi et al., 2019), and Pd (Khodaei and Dehghan, 2019; Esmailpour and Zahmatkesh, 2019; Mhaldar et al., 2020; Vibhute et al., 2020; Sarkar et al., 2015; Alamgholiloo et al., 2020). Of these, Pd-catalyzed cross-coupling reactions are the most effective synthetic route and have been studied extensively by researchers. In general, the catalytic activity of solid supported heterogeneous metal catalysts is not as efficient as that of homogeneous counter-catalysts due to their larger surface area and smaller centres (Bodaghifard, 2019). However, due to high prices and toxicity of the metal palladium, it is necessary to develop simple and inexpensive highly reactive heterogeneous-Pd catalysts (Lim and Lee, 2010; Garrett and Prasad, 2004) to minimize of palladium contamination and its harmful effects to the environment and reduce costs. From an economic, sustainable and ecological point of view, it is of great important to develop a highly active, reusable Pd-catalyst that prevents the loss of small amounts of metal and which can also be easily recovered from the reaction mixture. Conventional heterogeneous catalysts have several disadvantages, such as low efficiency, stability and metal bonding ability, and require high temperatures and harsh reaction conditions. An interesting approach to overcome these disadvantages is the immobilization of metal catalysts on nanoparticle-based solid supports, which provides an accumulation of advantages of both homo- and heterogeneous metal catalysts (Mofijur et al., 2020; Hong et al., 2020; Ahadi et al., 2019; Algarou et al., 2020). Palladium nanoparticles have attracted immense interest in the academic and industrial research field of fabrication because of their superior reactivity due to their huge surface area, which greatly improves the interaction of reactant and the catalytic active sites of the metal (Isfahani et al., 2013).

Therefore, a useful approach is the stabilization of a metal catalyst on a solid support, which increase the surface area,

provides the properties of nanoparticles with a large number of active catalytic centres and facilitates agglomeration and prevents their coherent distribution (Yang et al., 2013; Li et al., 2013; Li et al., 2012). In recent years, much effort has been put into introducing a different catalyst that is more efficient, environmentally friendly, easier and more reliable by introducing palladium nanoparticles on a solid support. For example, carbon-based materials (Sun et al., 2013; Kamal et al., 2012; Shekarizadeh and Azadi, 2020), cellulose (Sarkar et al., 2017), silica (Sarkar et al., 2015), polymers (Sato et al., 2015), magnetic Fe_3O_4 (Choghamarani et al., 2019; Vinnik et al., 2021); MOF (Luo et al., 2019; Van Velthoven et al., 2020); carbon nanotubes (Zhou et al., 2017) composite materials (Madrahalli Bharamanagowda et al., 2020), Pd-NHCs complex in MIL-101 (Cr) (Niknam et al., 2021); fiber (Xiao et al., 2021) were investigated for the development of stabilized nanocatalysts based on palladium. However, they suffer from limitations such as high cost, the use of toxic solvents throughout catalyst preparation, and high consumption of chemicals.

Among the various nanoparticles, magnetite (Fe_3O_4) widely used as a solid support for palladium (Fatahi et al., 2021; Marandi and Koukabi, 2021) due to its unique physicochemical properties, low cost, non-hazardous, high chemical and thermal stability, and biocompatibility (Arco et al., 2016) and easy separation from the reaction mixture (Firouzabadi et al., 2014; Ma et al., 2018; Trukhanov et al., 2021). One of the issues associated with Fe_3O_4 nanoparticles is their poor stability, specifically under acidic conditions. This is because it aggregates over time to reduce surface area and tends to oxidize easily in normal atmospheres (Corma, 1997). To overcome these problems, efficient methods are needed for the preparation of nanoparticles that enhance their physicochemical stability against degradation in the course of or after the synthesis process. Recently, silicon dioxide has been used as a protective shell of Fe_3O_4 , which can (1) inhibit the aggregation and formation of Fe_3O_4 (2) keeping the magnetic properties of the core with efficient separation for reuse (3) provides large surface Si-OH groups for further modifications and (4) well-defined distribution of active metal centres or intrinsic acid-basic reactive centres to forward the catalytic reaction smoothly (Du et al., 2012; Li et al., 2013).

This study introduces a recyclable silica-coated superparamagnetic iron oxide-based shift-based $\text{Fe}_3\text{O}_4@\text{SiNSB-Pd}$ nanocatalyst and its catalytic application toward Mizoroki-Heck C-C bond formation reactions. The $\text{Fe}_3\text{O}_4@\text{SiNSB-Pd}$ effectively facilitated Mizoroki-Heck and Heck-Matsuda reactions of arene halides and arene-diazonium salts with various olefins to give the corresponding olefinic products in excellent yields. The cross-coupling results indicated that the supported $\text{Fe}_3\text{O}_4@\text{SiNSB-Pd}$ propagated the reaction efficiently and could be recovered from the reaction combination using an external magnet. The $\text{Fe}_3\text{O}_4@\text{SiNSB-Pd}$ was successfully reused seven-times without any significant drop of its initial catalytic activity.

2. Experimental

2.1. Preparation of Fe_3O_4 nanoparticles

To a 300 ml beaker, 6.5 g of $\text{FeCl}_3 \cdot 6\text{H}_2\text{O}$ and 2.43 g sodium citrate were dissolved in 75 ml of ethylene glycol for 1 h with vig-

orous magnetic stirring. To this solution, 12 g of NaOAc was added and the mixture was aggressively stirred for another 1 h. The reaction mixture was heated for 8 h at 200 °C in a Teflon-lined stainless-steel autoclave. After that, the autoclave was left to cool to ambient temperature naturally. A magnet was used to collect the black Fe₃O₄ magnetic nanoparticles (MNPs), which were then rinsed multiple times with an aqueous solution of ethanol before being oven-dried at 60 °C overnight.

2.2. Synthesis of silica coated [Fe₃O₄@Si] 1

A modified Stöber method was used to cover the SiO₂ layer on Fe₃O₄ nanoparticles. In a typical synthesis process of core-shell Fe₃O₄@Si, 1 g of as-prepared Fe₃O₄ particles were added to a round-bottom flask and the particles were sonicated for 1 h. To this suspension, a mixture of 350 ml ethanol, 85 ml of deionized water, and 6 ml of concentrated ammonia were added. The resulting mixture was stirred and 3 ml of TEOS was added dropwise to the reaction flask and continued to stir for 6 h at room temperature. The magnetically coated [Fe₃O₄@Si] 1 product was washed with aqueous ethanol, dried at 60 °C and separated by using of an external magnet.

2.3. Amine functionalization [Fe₃O₄@Si-NH₂] 2

The amine functionalized Fe₃O₄@Si-NH₂ was synthesized by post-synthesis grafting method. The synthesized silica coated 1 (6 g) was dispersed in 45 ml of toluene for 10 min at 50 °C. Then to this suspension, 4 ml of 3-aminopropyltriethoxysilane (APTES) was added and the reaction mixture was refluxed for 12 h. The amino functionalized magnetic solid products were filtered off, washed several times with methanol and dried at 70 °C for 12 h. The magnetic [Fe₃O₄@Si-NH₂] 2 was separated using an external permanent magnet (Fekri and Zeinali, 2020).

2.4. Preparation of magnetic Schiff-base [Fe₃O₄@SiNSB] 3

The amine functionalized [Fe₃O₄@SiO₂-NH₂] 2 (1 g) was dispersed in 30 ml of ethanol and 1 mmol of 1,10-phenanthroline-2,9-dicarbaldehyde was added to the reaction mixture. The resulting suspension was stirred at 60 °C for 12 h under a nitrogen atmosphere. The reaction mixture was cooled to room temperature, and the resulting 3 was filtered on a glass filter, washed three times with ethanol and dried in oven at 60 °C.

2.5. Preparation of [Fe₃O₄@SiNSB-Pd] 4

An aqueous solution of (NH₄)₂PdCl₄ (280 mg, 45 ml of water) was added to a stirred suspension of [Fe₃O₄@SiNSB] 3 (1.5 g) in 50 ml of methanol. The resulted suspension was stirred at 25 °C for 1 h, and 0.75 ml of hydrazine monohydrate was added. The lite brown colour Fe₃O₄@SiNSB turned to dark brown and the mixture was continued to stir for another 1 h at 25 °C. The resulted magnetic silica coated palladium nanocatalyst [Fe₃O₄@SiNSB-Pd] 4 was filtered on a glass filter, washed with aqueous MeOH and dried in oven at 60 °C for 2 h. ICP-AES analysis of 4 showed 0.015 mmol/g of palladium was contained and the average Pd-nanoparticle 3.5 ± 0.6 nm was determined by TEM analysis.

2.6. Procedure for cross-coupling reaction

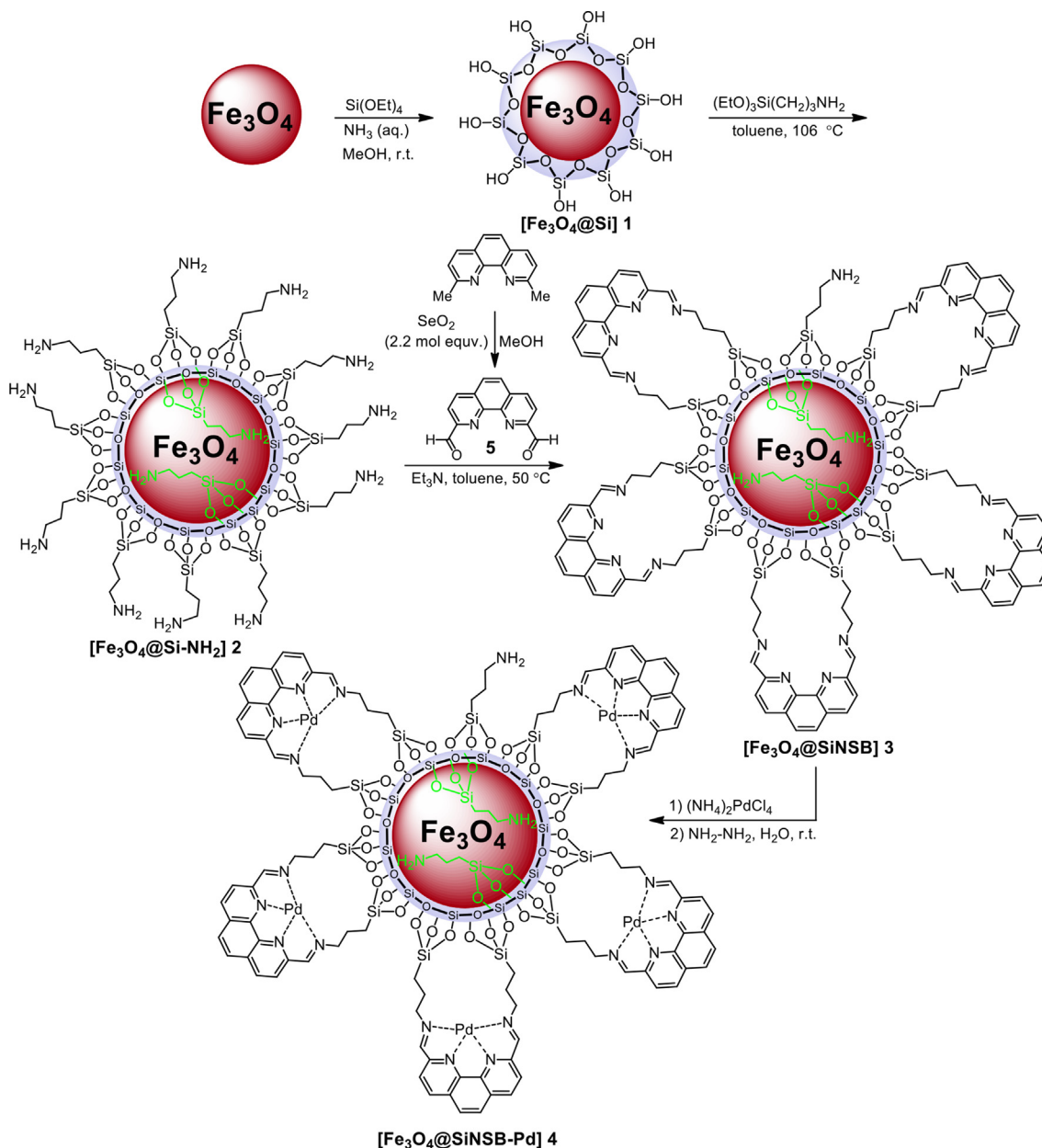
A 10 ml screw-cap glass vial was charged with 10 mg (0.00015 mmol 0.015 mol%) of 4, aromatic halide (1.0 mmol), olefine (1.5 mmol), Et₃N (3 mmol) and 2 ml of DMA. The reaction vial was heated at 130 °C for 6 h. For Heck-Matsuda reaction, we just added catalyst, arenediazonium salt, olefine in ethanol and stirred at room temperature for 5 h. The reaction progress and the production of cross-coupling product was monitored by TLC and GC analyses. After completion of the reaction, the reaction vial was cold to room temperature, diluted with ethyl acetate and the solid 4 was separated with an external magnet. The organic layer was washed with water, dried over MgSO₄ and the volatile materials were removed under reduced pressure. The crude product was purified on a short silica gel column chromatography using hexane and ethyl acetate as an eluent. ¹H NMR for 6a: 500 MHz δ 7.67 (d, 1H, J = 16.0 Hz), 7.43 (d, 2H, J = 8.15 Hz), 7.19 (d, 2H, J = 8.0 Hz), 6.41 (d, 1H, J = 16.0 Hz), 4.20 (t, 2H, J = 6.75 Hz), 2.37 (s 3H), 1.71–1.66 (m 2H), 1.46–1.43 (m 2H), 0.96 (t, 3H, J = 7.45 Hz). ¹³C NMR (125 MHz) δ 144.52, 140.58, 131.72, 129.57, 128.02, 117.18, 64.32, 30.77, 21.42, 19.18, 13.73.

3. Results and discussion

The magnetic nanocatalyst was constructed based on the incorporation of palladium nanoparticles onto a silica coated Fe₃O₄ core-shell phenanthroline Schiff base structure. The synthesis steps for nanocatalyst are schematically illustrated in Scheme 1. Preparation of the Fe₃O₄ was carried out by the reaction of Fe³⁺ with an aqueous solution of sodium acetate, sodium citate in ethylene glycol at 200 °C. After successfully synthesis of magnetic Fe₃O₄ nanoparticles, SiO₂ encapsulation was accomplished using tetraethylorthosilicate (TEOS) in aqueous ammonia solution. The resulted 1 core-shell was then treated with (3-aminopropyl)triethoxysilane (APTES) to afford amino functionalized 2. To introduce phenanthroline chelating group onto the amino functionalized nanoparticles 2 first we treated 2,9-dimethyl-1,10-phenanthroline with selenium oxide (Johnson and Ji, 2018) to afford the corresponding dialdehyde 5 and the respective ¹H NMR spectrum is presented in Fig. 1.

This dialdehyde 5 was then treated with 2 at 50 °C in toluene to give the corresponding phenanthroline Schiff base 3 and it has been used as Schiff base magnetic bidentate chelating ligand to the incorporation of palladium nanoparticles. To obtain the magnetically silica coated Schiff-based palladium nanocatalyst we treated 3 with an aqueous solution of ammonium tetrachloropalladate at room temperature. The resulting brown colored palladium complex was then treated with hydrazine hydrate to produce the nanocatalyst 4 as a dark brown solid powder. The content of palladium in the nanocatalyst 4 was 0.015 mmol/g. The synthesized material and the composition of the nanocatalyst 4 were examined using various spectroscopic methods.

The FT-IR spectra for all synthesized materials are represented in Fig. 2. Vibration at 3037 cm⁻¹ was associated with sp³ C-H stretching in 1 due to the entrapment of TEOS. After incorporating amino functionality in 1, the peaks of absorption were observed at 2850 cm⁻¹ and 2955 cm⁻¹ due to the ali-



Scheme 1 Synthesis of magnetically supported palladium nanocatalyst **4**.

phatic C-H (sp^3) stretching. The peaks at 3333 cm^{-1} and 3366 cm^{-1} were observed (N-H stretching) for primary amine group attached onto **2**. While, after incorporation of the phenanthroline chelating ligand onto **3** absorption peaks at 2845 cm^{-1} , 2955 cm^{-1} and 2993 cm^{-1} were observed and N-H stretching peaks were disappeared. Furthermore, after metallic palladium coordination with the nitrogen atoms, the IR peaks were shifted toward the shorter wave number and 2856 cm^{-1} , 2932 cm^{-1} , 2956 cm^{-1} and 3042 cm^{-1} peaks were observed for **4**.

The SEM image analysis of Fe_3O_4 showed that the synthesized magnetic nanoparticles were in spherical shape, well dispersed (Fig. 3a) and average diameter was 150 nm (Fig. 3b). SEM image of silica encapsulated core-shell **1** was also showed spherical morphology (Fig. 3c) and the magnified SEM image of **1** clearly indicated the successful encapsulation of Fe_3O_4

nanoparticles by silica (Fig. 3d). After incorporation of amino group with silanol moieties in **1**, the SEM image of **2** showed greater diameter than **1** (Fig. 3e). Due to the incorporation of the organic phenanthroline chelating group with **2**, the SEM image of **3** showed similar spherical structure with larger diameter than **2** (Fig. 3f). After introduction of palladium nanoparticles, the SEM image of **4** also showed rough morphologies on spherically shaped structures (Fig. 3g).

TEM image of **4** showed that the palladium nanoparticles were well dispersed onto the surface of Fe_3O_4 and the spherical shape of Fe_3O_4 nanoparticles were still maintained (Fig. 4a). The magnified TEM image of palladium nanoparticles in **4** were also showed spherical structure (Fig. 4b). About one hundred and twenty-five palladium nanoparticles were considered to determine the average diameter (Fig. 5) which was determined to be $3.5 \pm 0.6\text{ nm}$. Interestingly, the TEM image of

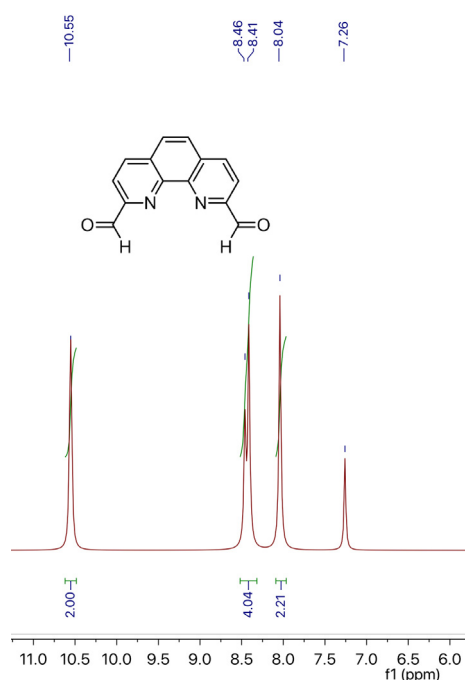


Fig. 1 ¹H NMR spectrum of 5.

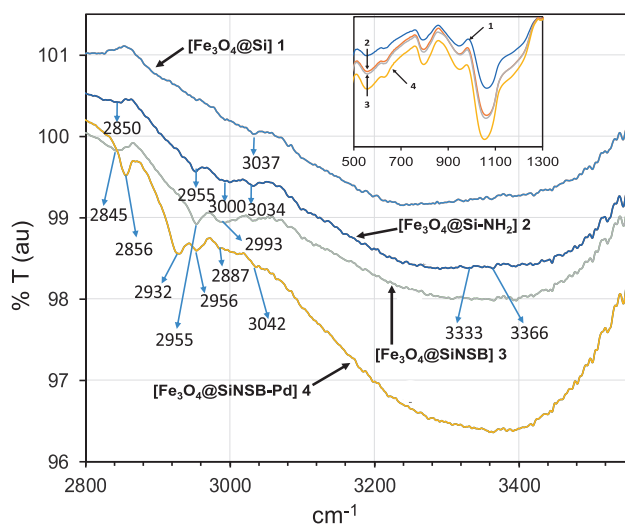


Fig. 2 FT-IR images of synthesized materials.

3rd recycle of **4** showed similar morphology with unused particles and were not aggregated after reused in the Heck reaction (Fig. 4c).

Fig. 6 showed a typical XRD diagram of Fe₃O₄, silica coated **1** and Schiff-based palladium nanocatalyst **4**. The six characteristic peaks $2\theta = 29.9$ (220), 36.3 (311), 43.6 (400), 53.5 (422), 57.5 (511) and 63.4 (440) were observed for the Fe₃O₄ nanoparticles. The crystallinity patterns of the Pd-nanoparticles indicate five distinct reflections at $2\theta = 40.2^\circ$ (111), 45.5° (200), 68.2° (220), 81.86° (311) and 86.12° (222) (Khan et al., 2014). These attribute reflections were considered to the face centered cubic (fcc) structure of palladium (JCPDS: 87-0641, space group: Fm3m (225)) (Shankar et al., 2004). The strong reflection at (111), in assessment with

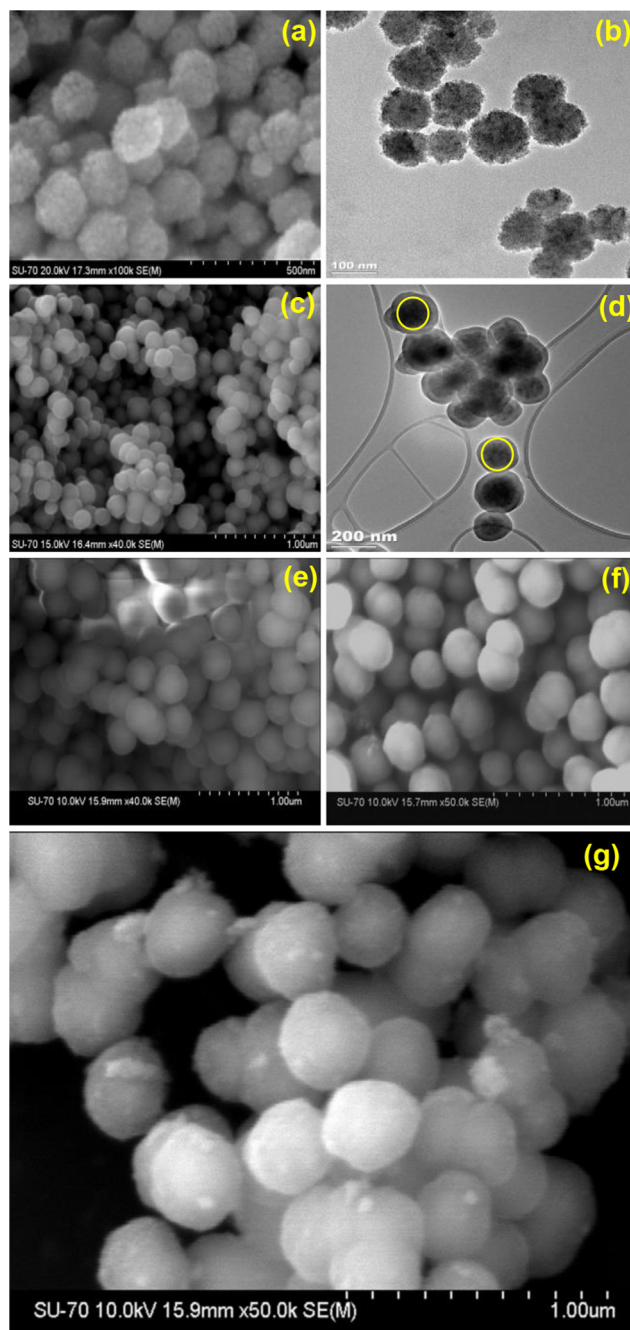


Fig. 3 (a) SEM image of Fe₃O₄, (b) nano scale SEM image of Fe₃O₄, (c) SEM image of **1**, (d) nano scale SEM image of **1**, (e) SEM image of **2**, (f) SEM image of **3**, (g) SEM image of **4**.

the other four, can be attributed to the desired growth controlled of the nanocrystals. On the basis of the half-width reflection at (111), the average crystallite size of Pd-nanoparticles (~ 3.56 nm) was determined using the Scherrer equation. The broad peak at 2θ of 20 – 28 corresponds to the amorphous structure of the silica layer (Safavi et al., 2013).

The X-ray photoelectron spectra (XPS) of **4** showed in Fig. 7. For comparison of the oxidation states of palladium, we measure XPS of **4** and (NH₄)₂PdCl₄. The narrow scan profile of **4** displayed two signals at 335.7 eV and 340.6 eV those

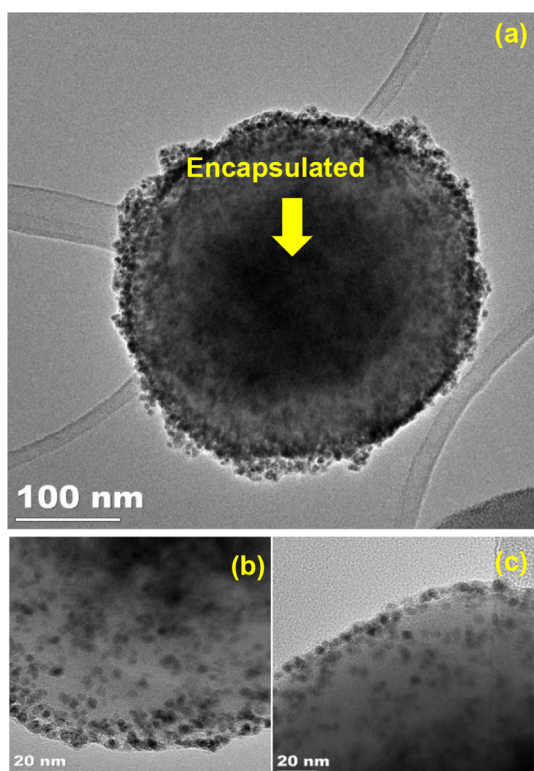


Fig. 4 (a) TEM image of **4**, (b) TEM image of magnified **4**, (c) TEM image of 3rd recycled of **4**.

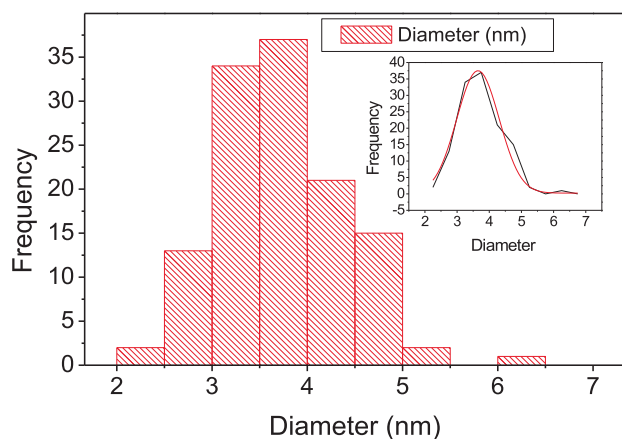


Fig. 5 Palladium nanoparticles size distribution of **4**.

can be assigned to $\text{Pd}3d_{5/2}$ and $\text{Pd}3d_{3/2}$ for Pd^0 species respectively (Zhang et al., 2017). However, signals at 337.52 eV and 342.82 eV were observed with respect to $\text{Pd}3d_{5/2}$ and $\text{Pd}3d_{3/2}$ for $\text{Pd}(\text{II})$ species in $(\text{NH}_4)_2\text{PdCl}_4$ which indicated that the palladium was successfully reduced by hydrazine.

After successfully characterization, the catalytic applicability of **4** to the Mizoroki-Heck C-C bond formation reaction was investigated. The nanocatalyst **4** was applied for the construction of C-C bond by the utilization of alkenes and arene halides to afford the corresponding substituted alkenes. Reactions were performed under various conditions to identify the

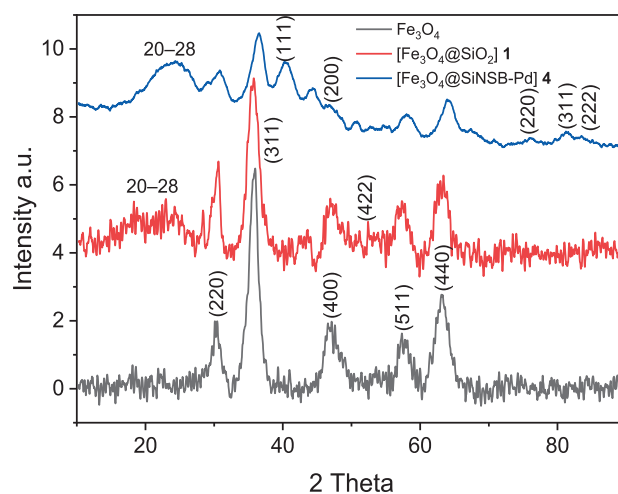


Fig. 6 XRD spectra of synthesized materials.

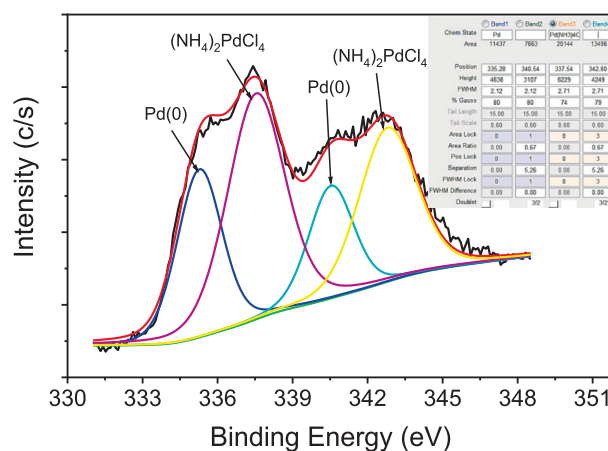
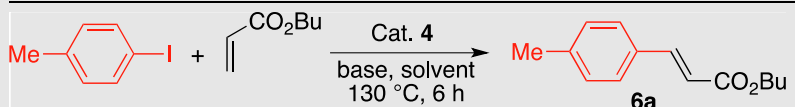


Fig. 7 Narrow scan XPS image of $\text{Pd}(0)$ in **4**.

optimal conditions for Heck C-C bond formation. The reaction of butyl acrylate and 4-iodotoluene was carried out using a fixed catalytic dose (10 mg, 0.015 mol%), temperature (130 °C) and reaction time (6 h) where solvents and bases were varied. It was found that the desired product was obtained under all reaction conditions (Table 1). The yields of the product were lower when aqueous DMF and inorganic bases were used (entries 1–4). However, the yield was significantly increased when organic bases *i.e.* triethyl amine and diisopropylethyl amine were used (entries 5–6). Interestingly, the best result was achieved when the Heck C-C bond formation reaction was conducted with triethyl amine in *N,N*-dimethylacetamide (entry 8). The reaction was also performed using 0.0075 mol% of **4** (entry 9) and 64% yield was obtained. However, NMP and DMSO were not found to be good solvents for this catalytic system. Therefore, suitable reaction conditions were considered to consist of DMA as solvent, triethyl amine as base, 0.015 mol% of **4** nanocatalyst at 130 °C for 6 h (Table 1, Entry 8).

After screening of the Heck C-C bond formation reaction, we extended the application of **4** to a variety of substituted arene halides and olefins (Table 2). An olefine *i.e.* methyl acry-

Table 1 Screening of the Heck reaction^a.


Entry	Solvent	Base	Yield (%) ^[b]
1	DMF:H ₂ O	Na ₂ CO ₃	71(67) ^[c]
2	DMF:H ₂ O	K ₂ CO ₃	66
3	DMF:H ₂ O	NaOMe	68
4	DMF:H ₂ O	Na ₃ PO ₄	70
5	DMF	DIPEA	85
6	DMF	Et ₃ N	91
7	DMA	DIPEA	86
8	DMA	Et ₃ N	95(91) ^[c]
9 ^d	DMA	Et ₃ N	71(64) ^[c]
10	NMP	Et ₃ N	84
11	DMSO	Et ₃ N	76

^[a]Reaction conditions: 4-iodotoluene (1 mmol), butyl acrylate (1.5 mmol), **4** (0.015 mol%), base 3 mmol and 2 ml of solvent for 6 h. ^[b]GC yields.

^[c]Isolated yield. ^[d]Reaction was conducted in presence of 0.0075 mol% of **4**.

late was smoothly reacted with 4-iodoanisole, iodobenzene and 3-iodotoluene to afford the respective alkenes **6b-d** with 92%, 94% and 92% yields respectively. The C-C bond formation reactions of arene bromides and olefins are in great demand because of the low cost of arene bromides, those are desirable material for industrial and pharmaceutical applications. By observing the excellent catalytic performance of **4** towards the arene iodides, we further investigated the scope of the Heck C-C bond formation reaction of electronically poor arene bromides with a variety of olefins. The nanocatalyst **4** showed excellent catalytic efficiency towards arene bromides and substituted arene bromides with a variety of olefins to afford the respective products **6b-d** with 87%, 86%, and 84% yields. It was observed that arene bromides showed lower catalytic activity compared to arene iodide due to the slow oxidative addition rate of arene bromides with the active site of metal catalyst in the catalytic cycle. A variety of olefins, such as butyl acrylate and *N*-isopropyl acrylamide, were also readily formed C-C bond with arene halides to provide the corresponding alkenes in excellent yield (**6e-j**). The highest yield of the corresponding product (**6g**) was observed in the couplings of 4-iodonitrobenzene and butyl acrylate. The arene halides having electron-rich group showed higher catalytic activity compared to the electron-poor arene halides. The arene bromides were also smoothly afforded the respective products **6e-j** in up to 85% yield. Interestingly, the sterically hindered, bulky and less reactive arene olefin *i.e.* styrene was also smoothly forwarded the Heck C-C bond formation reaction with arene halides to produce the corresponding stilbene derivatives **6k-m** in high yield. Recently, Yamada et. al (Yamada et al., 2014) reported that palladium nanoparticles on silicon nanowire (SiNA-Pd, 0.3 mol%) catalyzed Heck C-C bond formation reaction at 140 °C in presence of 0.2–1 mol equiv of tetrabutylammonium bromide as an additive and they continued the reaction for 48 h which provided only 85% yield of **6f**. Herein our catalytic system showed twenty times more reactive compared to their work.

We further extended the catalytic applicability of **4** to the Heck-Matsuda C-C bond formation reaction of arenediazonium salt which is known as an excellent arene electrophile.

(Andrus et al., 2002; Selvakumar et al., 2002). To investigate the catalytic efficiency of **4**, 4-methoxyarenediazonium tetrafluoroborate was treated with methyl acrylate at room temperature for 5 h smoothly afforded the respective cross-coupling product **6b** with 92% yield (Table 3). It is known that arene diazonium salt easily form an active cationic arene-Pd (II) species through oxidative addition during the catalytic cycle which enhance the rate of formation of product (Penafiel et al., 2012). Therefore, the Heck-Matsuda C-C bond formation can be carried out under mild reaction conditions compared to the traditional Mizoroki-Heck reaction. When phenyldiazonium salt was treated with olefine *i.e.* methyl acrylate the C-C bond formation reaction smoothly forwarded to give **6c** in 91% yield. The electron pushing and electron withdrawing substituted arene diazonium salts were efficiently forwarded the Heck-Matsuda reaction with butyl acrylate to afford the respective cross-coupling products **6a**, **6n** and **6g** with 87%, 88% and 93% yield respectively. *N*-isopropylacrylamide is relatively less reactive compared to methyl or butyl acrylate however *N*-isopropylacrylamide was also smoothly promoted Heck-Matsuda reaction to afford the respective products **6g** and **6i** in 86% and 83% yield respectively. Interestingly the coupling of sterically hindered styrene and aromatic diazonium salts was also observed under reaction conditions at room temperature and the yields of the corresponding coupling products **6l** and **6m** were 89% and 88%, respectively.

The current catalyst is compared between the previously reported catalyst to evaluate the performance and applicability of the developed catalyst **4**. For improved comparison, the results of the iodobenzene in the Heck reaction was selected and the time of product formation and catalyst loading were compared with the catalyst mentioned earlier in Table 4 (Li et al., 2018; Naghipour and Fakhri 2016; Banazadeh et al., 2015; Wang et al., 2006; Nasrollahzadeh et al., 2014; Wang et al., 2014; Zhang et al., 2011; Zolfigol et al., 2014). The catalyst used in this Heck C-C bond formation reactions does not have serious issues such as high acceleration, large dosage, low catalytic efficiency, high reaction temperature, and longer reaction time. In addition, the reusability and recycling of this new

Table 2 Heck reaction of arene halides^a.

<p>6b: X = I, 92% Br, 87%</p>	<p>6c: X = I, 94% Br, 86%</p>	<p>6d: X = I, 92% Br, 84%</p>
<p>6e: X = I, 90% Br, 82%</p>	<p>6f: X = I, 92% Br, 83%</p>	<p>6g: X = I, 95% Br, 87%</p>
<p>6h: X = I, 88% Br, 79%</p>	<p>6i: X = I, 87% Br, 80%</p>	<p>6j: X = I, 85% Br, 78%</p>
<p>6k: X = I, 89% Br, 81%</p>	<p>6l: X = I, 87% Br, 81%</p>	<p>6m: X = I, 86% Br, 76%</p>

^aReaction condition: arene halide (1 mmol), alkene (1.5 mol equiv), 0.015 mol% of **4**, Et₃N 3 mmol, 2 ml of DMA.

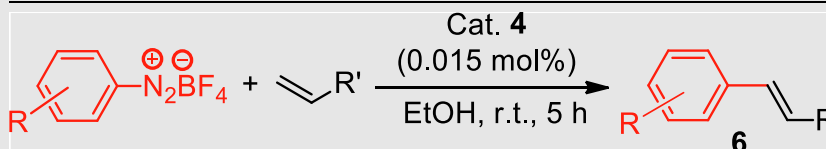
catalyst is more convenient and faster than those previously reported. In addition, the small catalyst (0.0075 mol%) of nanocatalyst **4** is another advantage of the current catalyst compared to others (Table 1, entry 9).

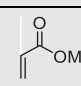
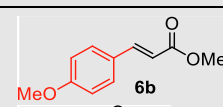
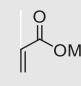
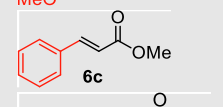
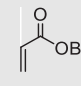
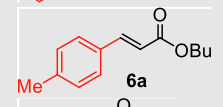
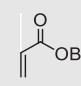
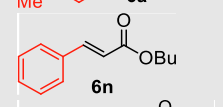
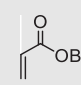
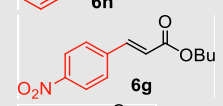
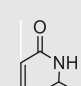
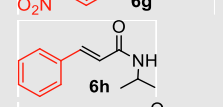
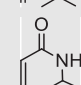
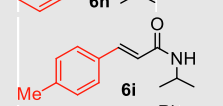
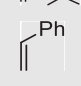
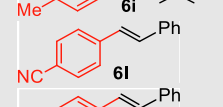
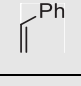
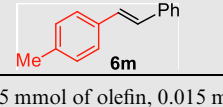
The reusability of the heterogeneous catalyst has significant interest from an economical and sustainable viewpoint. Therefore the recoverability and potential reuse of nanocatalyst **4** was investigated. After the first cycle of Heck reactions (Table 2, **6g**, X = I), a strong magnet was applied outside of the reaction vessel and carefully remove the reaction mixture (Fig. 8).

The magnetic nanocatalyst was cleaned with ethyl acetate, dried at 50 °C for 30 min and used it to the next catalytic cycle. The magnetically recyclable and separable palladium nanocatalyst **4** was repeatedly used seven times and found excellent

catalytic performance with no significant drop in its catalytic performance. A slight decrease of catalytic performance has been seen due to loss of **4** during its recovery process (Fig. 9). The TEM image of 3rd recycles of **4** is presented in Fig. 4c which clearly indicated that after the Heck reaction, palladium nanoparticles were not aggregated. Therefore, silica coated magnetic phenanthroline based palladium nanocatalyst **4** exhibited high stability and catalytic performance in the cross-coupling reactions.

Heterogeneous catalysts have an important aspect in the stability and heterogeneity of the supported metal catalyst during the reaction. Therefore, a thermal filtration experiment was conducted to evaluate whether the reaction would proceed under the conditions of a heterogeneous reaction (Fig. 10). We considered the hot filtration experiment using **4**

Table 3 Heck-Matsuda cross-coupling^a.


Entry	Olefin	Product	Yield (%) ^b
1			92
2			91
3			87
4			88
5			93
6			86
7			83
8			89
9			88

^aReaction condition: 1 mmol of arenediazonium tetrafluoroborate, 1.5 mmol of olefin, 0.015 mol% **4**, 3 ml of ethanol, 5 h at r.t. ^bIsolated yield.

Table 4 Catalytic efficiency comparison of [Fe₃O₄@SiNSB-Pd] **4** with previously reported in the Heck reaction.

Catalyst	Conditions	Time (h)	Yield (%)	Ref.
0.1-PdAu0.16/Fe ₃ O ₄ @LDH, (0.05 %)	DMF/H ₂ O, K ₂ CO ₃ , 120 °C	1.5	89.7	(Li et al., 2018)
Fe ₃ O ₄ @CS-Schiff base, (1 %)	DMF, Et ₃ N	0.3	98	(Naghypour and Fakhri, 2016)
Fe ₃ O ₄ @(A-V)-silica-PdMNPs, (0.4%)	K ₂ CO ₃ , DMF, 130 °C.	2.5	95	(Banazadeh et al., 2015)
MNPs-TDA-Pd (20 mg)	K ₂ CO ₃ , DMF, 100 °C,	8 h	93	(Bodaghifard, 2019)
Fe ₃ O ₄ @SiO ₂ -HPGOPPh ₂ -PNP, (25 mg)	K ₂ CO ₃ , DMF, 100 °C,	1 h	87	(Du et al., 2012)
Fe ₃ O ₄ @SiO ₂ -NH ₂ -Pd (30 mg)	CH ₃ CN/H ₂ O, NaOAc, reflux	12 h	71	(Wang et al., 2006)
TiO ₂ @Pd NPs (1%)	DMF, Et ₃ N, 140 °C	10	93	(Nasrollahzadeh et al., 2014)
HMMS-NH ₂ -Pd (4%)	NMP, K ₂ CO ₃ , 130 °C	8	98	(Wang et al., 2014)
Fe ₃ O ₄ -NH ₂ -Pd (5%)	NMP, K ₂ CO ₃ , 130 °C	10	99	(Zhang et al., 2011)
SMNPs-DF-Pd (1%)	Solvent free, DABCO, 140 °C	2	92	(Zolfigol et al., 2014)
Fe ₃ O ₄ @SiNSB-Pd (0.015%)	DMA, Et ₃ N, 130 °C	6	94	This report

iodotoluene with butyl acrylate under optimized reaction conditions (Table 1, entry 8). After two hours of reaction, the magnetic nano catalyst was removed with an external magnet under hot conditions and the reaction vial was heated again under the same reaction conditions.

Interestingly, the Heck C-C bond formation reaction was not preceded even 5 h after removing of the catalyst. In addition, ICP-AES analysis of the filtrate showed no palladium specie was leached out into the reaction mixture. Thus, it is reasonable to state that the Heck C-C bond formation

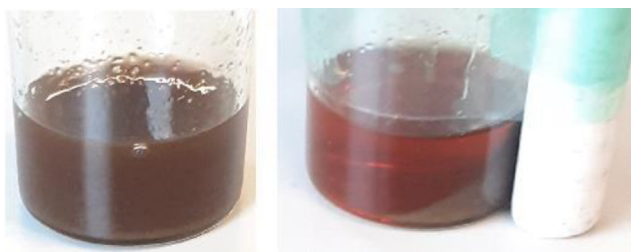


Fig. 8 Recovery of **4** by using external magnet.

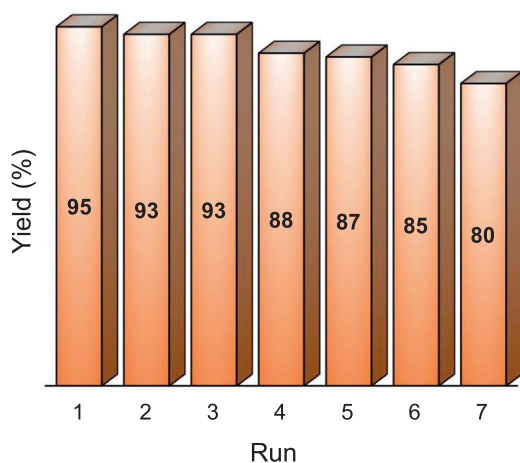


Fig. 9 Recycle of **4**.

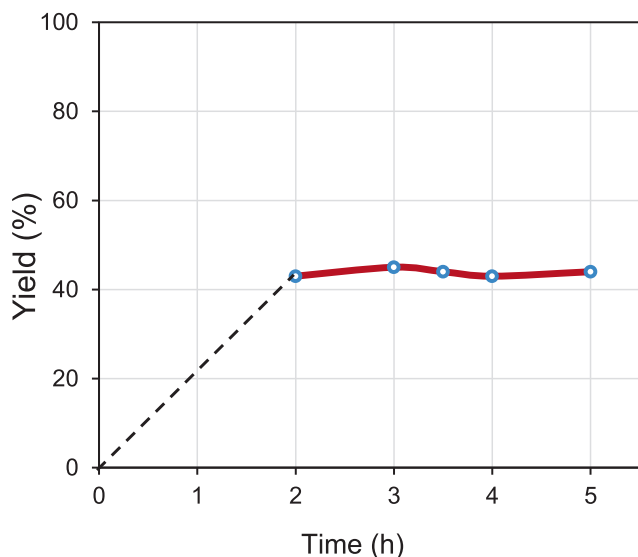


Fig. 10 Heterogeneity test of **4** in the Mizoroki-Heck reaction.

reactions were proceed under heterogeneous metal catalysed conditions.

4. Conclusions

In summary, we have successfully synthesized and characterized a recyclable palladium nanocatalyst based on

silica-coated magnetic core shell phenanthroline. The magnetic palladium nanocatalyst was well stabilized by the phenanthroline ligand and showed excellent catalytic performance in the Mizoroki-Heck C-C bond formation reaction of arene iodides/bromides with various types of olefins to provide the corresponding olefinic products in excellent yield. The magnetic catalyst was also efficiently promoted Heck-Matsuda C-C bond formation reaction of arene diazonium tetrafluoroborate salts with a variety of olefins to afford the respective olefinic products at room temperature. The magnetic palladium nanocatalyst showed high stability in the reaction medium and it was easy to recover from the reaction mixture with an external magnet. Moreover, the heterogeneous nanocatalyst could be reused in seven consecutive cycles without significant decrease of initial catalytic efficiency.

Declaration of Competing Interest

The authors declare that they have no known competing financial interests or personal relationships that could have appeared to influence the work reported in this paper.

Acknowledgments

The authors are thankful to the Research Management Centre of Universiti Malaysia Sabah for support to this work.

Appendix A. The NMR spectra for the synthesized coupling products can be found in the supplementary information section.

Appendix B. Supplementary material

Supplementary data to this article can be found online at <https://doi.org/10.1016/j.arabjc.2022.103914>.

References

- Trost, B.M., Knopf, J.D., Brindle, C.S., 2016. *Chem. Rev.* 116, 15035.
- Biffis, A., Centomo, P., Zotto, A.D., Zecca, M., 2018. *Chem. Rev.* 118, 2249.
- Arghan, M., Koukabi, N., Kolvari, E., 2018. *Appl. Organo Chem.* 32, 4346.
- Parouch, A.N., Koukabi, N., Abdous, E., 2020. *Res. Chem. Intermed.* 46, 3295.
- Das, P., Bora, U., Tairai, A., Sharma, C., 2010. *Tetrahedron Lett.* 51, 1479.
- Sardarian, A.R., Kazemnejadi, M., Esmailpour, M., 2019. *Dalton Trans.* 48, 3132.
- Parlett, C.M.A., Wilson, K., Lee, A.F., 2013. *Chem. Soc. Rev.* 42, 3876.
- Veerakumar, P., Thanasekaran, P., Lu, K.L., Lin, K.C., Rajagopal, S., Sustain, A.C.S., 2017. *Chem. Eng.* 5, 8475.
- Polshettiwar, V., Luque, R., Fihri, A., Zhu, H., Bouhrara, M., Basset, J.M., 2011. *Chem. Rev.* 111, 3036.
- Esmailpour, M., Javidi, J., Nowroozi Dodeji, F., Mokhtari Abarghoui, M., 2014. *J. Mol. Catal. A Chem.* 393, 18.
- Calo, V., Nacci, A., Monopoli, A., Ieva, E., Cioffi, N., 2005. *Org. Lett.* 7, 617.
- Zheng, Y.L., Newman, S.G., 2019. *Angew. Chem. Int. Ed.* 58, 18159.

- Kazemnejadi, M., Alavi, S.A., Rezazadeh, Z., Nasser, M.A., Allahresani, A., Esmailpour, M., 2019. *Green Chem.* 21, 1718.
- Khodaei, M.M., Dehghan, M., 2019. *Appl. Organomet. Chem.* 33, 4618.
- Esmailpour, M., Zahmatkesh, S., 2019. *Inorg. Nano-Met Chem.* 49, 267.
- Mhaldar, P., Vibhute, S., Rashinkar, G., Pore, D., 2020. *React. Funct. Polym.* 152, 104586.
- Vibhute, S.P., Mhaldar, P.M., Shejwal, R.V., Rashinkar, G.S., Pore, D.M., 2020. *Tetrahedron Lett.* 61, 151801.
- Sarkar, S.M., Rahman, M.L., Yusoff, M.M., 2015. *RSC Adv.* 5, 19630.
- H. Alamgholilo, S. Rostamnia, N. Noroozi Pesyan, *Appl. Organomet. Chem.* 2020, 34, 5452.
- Bodaghifard, M.A., 2019. *J. Organomet. Chem.* 886, 57.
- Lim, C.W., Lee, I.S., 2010. *Nano Today* 5, 412.
- Garrett, C.E., Prasad, K., 2004. *Adv. Synth. Catal.* 346, 889.
- Mofijur, M., Siddiki, S.Y.A., Ahmed, M.B., Djavanroodi, F., Fattah, I.R., 2020. *H. C. Chemosphere* 128642.
- Hong, K., Sajjadi, M., Suh, J.M., Zhang, K., Nasrollahzadeh, M., Jang, H.W., Varma, R.S., Shokouhimehr, M., *Appl. A.C.S.*, 2020. *Nano Mater.* 3, 2070.
- Ahadi, A., Rostamnia, S., Panahi, P., Wilson, L.D., Kong, Q., An, Z., Shokouhimehr, M., 2019. *Catalysts* 9, 140.
- Algarou, N.A., Slimani, Y., Almessiere, M.A., Alahmari, F.S., Vakhitov, M.G., Klygach, D.S., Trukhanov, S.V., Trukhanov, A. V., Baykal, A., 2020. *J. Mater. Res. Technol.* 9, 5858–5870.
- Isfahani, A.L., Baltork, I.M., Mirkhani, V., Khosropour, A.R., Moghadam, M., Tangestaninejad, S., Kia, R., 2013. *Adv. Synth. Catal.* 355, 957.
- Yang, J., Wang, D., Liu, W., Zhang, X., Bian, F., Yu, W., 2013. *Green Chem.* 15, 3429.
- Li, W., Zhang, B., Li, X., Zhang, H., Zhang, Q., 2013. *Appl. Catal. A Gen.* 459, 65.
- Li, H., Wang, L., Yang, M., Qi, Y., 2012. *Catal. Commun.* 17, 179.
- Sun, W., Liu, Z., Jiang, C., Xue, Y., Chu, W., Zhao, X., 2013. *Catal. Today* 212, 206.
- Kamal, A., Srinivasulu, V., Seshadri, B.N., Markandeya, N., Alarifi, A., Shankaraiah, N., 2012. *Green Chem.* 14, 2513.
- Shekarizadeh, A., Azadi, R., 2020. *Appl. Organomet. Chem.* 34, 5775.
- Sarkar, S.M., Rahman, M.L., Chong, K.F., Yusoff, M.M., 2017. *J. Cat* 350, 103–110.
- Sarkar, S.M., Yusoff, M.M., Rahman, M.L., 2015. *J. Chin. Chem. Soc.* 62, 33–40.
- Sato, T., Ohno, A., Sarkar, S.M., Uozumi, Y., Yamada, Y.M.A., 2015. *ChemCatChem* 7, 2141–2148.
- Vinnik, D.A., Zhivulin, V.E., Sherstyuk, D.P., Starikov, A.Y., Zuzina, P.A., Gudkova, S.A., Zherebtsov, D.A., Rozanov, K.N., Trukhanov, S.V., Astapovich, K.A., Turchenko, V.A., Sombra, A.S.B., Zhou, D., Jotania, R.B., Singh, C., Trukhanov, A.V., 2021. *Mater. Today Chem.* 20, 100460.
- Choghamarani, A.G., Tahmasbi, B., Hudson, R.H.E., Heidari, A., 2019. *Micropor. Mesopor. Mat.* 284, 366.
- Van Velthoven, N., Henrion, M., Dallenes, J., Krajnc, A., Bugaev, A. L., Liu, P., Bals, S., Soldatov, A.V., Mali, G., De Vos, D.E., 2020. *ACS Catal.* 10, 5077.
- Luo, S., Zeng, Z., Zeng, G., Liu, Z., Xiao, R., Chen, M., Tang, L., Tang, W., Lai, C., Cheng, M., Shao, B., Liang, Q., Wang, H., Jiang, D., *Appl. A.C.S.*, 2019. *Mater. Inter.* 11, 32579.
- Zhou, A., Guo, R., Zhou, J., Dou, Y., Chen, Y., Li, J., Sustain, A.C.S., 2017. *Chem. Eng.* 6, 2103.
- M. Madrahalli Bharamanagowda, R. K. Panchangam, *Appl. Organomet. Chem.* 2020, 34, 5837.
- Niknam, E., Panahi, F., Nezhad, A.K., 2021. *Organomet. Chem.* 935, 121676.
- Xiao, J., Zhang, H., Ejike, A.C., Wang, L., Tao, M., Zhang, W., 2021. *React. Funct. Poly.* 161, 104843.
- Marandi, A., Koukabi, N., 2021. *Colloids Surf A Physicochem Eng Asp.* 621, 126597.
- Fatahi, Y., Ghaempanah, A., Mamani, L., Mahdavi, M., Bahadorikhalil, S., 2021. *J. Organomet. Chem* 936, 121711.
- Arco, L.R., Rodriguez, I.A., Carriel, V., Espinosa, A.B.B., Campos, F., Kuzhir, P., Duran, J.D.G., Lopez, M.T.L., 2016. *Nanoscale* 8, 8138.
- S. V. Trukhanov, T. I. Zubar, V. A. Turchenko, An. V. Trukhanov, T. Kmjec, J. Kohout, L. Matzui, O. Yakovenko, D. A. Vinnik, A. Yu. Starikov, V. E. Zhivulin, A. S. B. Sombra, D. Zhou, R. B. Jotania, C. Singh, A. V. Trukhanov, *Mater. Sci. Eng. B* 2021, 272, 115345.
- Firouzabadi, H., Iranpoor, N., Gholinejad, M., Akbaria, S., Jeddib, N., 2014. *RSC Adv.* 4, 17060.
- Ma, R., Yang, P.B., Bian, F.L., 2018. *New J. Chem.* 42, 4748.
- Corma, A., 1997. *Chem. Rev.* 97, 2373.
- Du, Q., Zhang, W., Ma, H., Zheng, J., Zhou, B., Li, Y., 2012. *Tetrahedron* 68, 3577.
- L. Z. Fekri, S. Zeinali. *Appl Organomet. Chem.* 2020, 5629.
- Johnson, N.M., Ji, H.F., 2018. *MOJ Biorg Org Chem.* 2, 154.
- Khan, M., Khan, M., Kuniyil, M., Adil, S.F., Warthan, A.A., Alkhatlan, H.Z., Tremel, W., Tahir, M.N., Siddiqui, M.R.H., 2014. *Dalton Trans.* 43, 9026.
- Shankar, S.S., Rai, A., Ankamwar, B., Singh, A., Ahmad, A., Sastry, M., 2004. *Nat. Mater.* 3, 482.
- Safavi, A., Banazadeh, A.R., Sedaghati, F., 2013. *Anal. Chim. Acta* 796, 115.
- Zhang, H., Yan, X., Huang, Y., Zhang, M., Tang, Y., Sun, D., Xu, L., Wei, S., 2017. *Appl. Surf. Sci.* 396, 812.
- Yamada, Y.M.A., Yuyama, Y., Sato, T., Fujikawa, S., Uozumi, Y., 2014. *Angew. Chem.* 126, 131.
- Selvakumar, K., Zapf, A., Spannenberg, A., Beller, M., 2002. *Chem. Eur. J.* 8, 3901.
- Andrus, M.B., Song, C., Zhang, J., 2002. *Org. Lett.* 4, 2079.
- Penafiel, I., Pastor, I.M., Yus, M., 2012. *Eur. J. Org. Chem.*, 3151
- Li, J., Wang, Y., Jiang, S., Zhang, H., 2018. *J. Organomet. Chem.* 878, 84.
- Naghypour, A., Fakhri, A., 2016. *Cat. Commun.* 73, 39.
- Banazadeh, A., Pirisedigh, A., Aryanasab, F., Salimi, H., Haghghi, S. S., 2015. *Inorg. Chim. Acta* 429, 132.
- Wang, Z., Xiao, P., Shen, B., He, N., 2006. *Colloids Surf. A Physicochem. Eng. Asp.* 276, 116.
- Nasrollahzadeh, M., Azarian, A., Ehsani, A., Khalaj, M., 2014. *J. Mol. Catal. A Chem.* 394, 205.
- Wang, P., Liu, H., Liu, M., Li, R., Ma, J., 2014. *New J. Chem.* 38, 1138.
- Zhang, F., Jin, J., Zhong, X., Li, S., Niu, J., Li, R., Ma, J., 2011. *Green Chem.* 13, 1238.
- Zolfigol, M.A., Azadbakht, T., Khakyzadeh, V., Nejatyami, R., Perrin, D.M., 2014. *RSC Adv.* 4, 40036.